

Supporting Information

Electronic Structure and Interfacial Microenvironment Engineering over Ni(OH)₂ Nanoarray for Boosted Electrocatalytic Upcycling of Polyethylene Terephthalate

*Xinci Hu^a, Wei Qiao^a, Yuxin Hu^a, Fengli Li^a, Yuting Yang^a, Zhihong Jiang^a, Yu Yu^b, Jingyun Fang^a,
and Ping Li^{a,*}*

^aSchool of Environmental Science and Engineering, Guangdong Provincial Key Laboratory of Environmental Pollution Control and Remediation Technology, Sun Yat-sen University, Guangzhou 510275, P. R. China

^bDepartment of Materials Science and Engineering, Beijing Jiaotong University, Beijing 100044, P. R. China

*E-mail: liping56@mail.sysu.edu.cn

Materials and reagents

The following chemicals were used as received without any further purification treatment: nickel nitrate hexahydrate [$\text{Ni}(\text{NO}_3)_2 \cdot 6\text{H}_2\text{O}$, $\geq 98\%$, Sinopharm], cobalt nitrate hexahydrate [$\text{Co}(\text{NO}_3)_2 \cdot 6\text{H}_2\text{O}$, 99.99%, Aladdin], hexamethylenetetramine (HMTA, $\geq 99\%$, Sinopharm), adipic acid [$\text{C}_6\text{H}_{10}\text{O}_4$, 99%, Aladdin], Sodium hypophosphite monohydrate ($\text{NaH}_2\text{PO}_2 \cdot \text{H}_2\text{O}$, 99%), N,N-dimethylformamide ($\text{C}_3\text{H}_7\text{NO}$, 99.9%, Aladdin), potassium hydroxide (KOH, $\geq 85\%$, Aladdin), ethylene glycol ($(\text{CH}_2\text{OH})_2$, 99%, Aladdin), formic acid (HCOOH , 99%, Aladdin), glycolic acid ($\text{C}_2\text{H}_4\text{O}_3$, $\geq 99\%$, Aladdin), ethanol ($\text{C}_2\text{H}_5\text{OH}$, AR, Guangzhou), hydrochloric acid (HCl , 36-38%, Guangzhou). Deionized water was collected by the Mill QHX 7040 purified water system.

Preparation of NF/CoP

The CoP nanosheet array was loaded on the NF substrate by hydrothermal reaction followed with phosphorization.¹ Firstly, the pretreated NF ($1 \times 3 \text{ cm}^2$) was immersed in a 25 mL of Teflon-lined stainless steel autoclave containing 15 mL of deionized water, 2 mmol of $\text{Co}(\text{NO}_3)_2 \cdot 6\text{H}_2\text{O}$, and 4 mmol of hexamethylenetetramine (HMTA). The autoclave was heated at 120 °C for 8 h and then cooled naturally to room temperature. After naturally cooled to the ambient temperature, the obtained NF/Co(OH)₂ was washed with deionized water and ethanol in sequence, and dried at 60 °C. Subsequently, the porcelain boat containing NF/Co(OH)₂ precursor and $\text{NaH}_2\text{PO}_2 \cdot \text{H}_2\text{O}$ was placed in the downstream and upstream of tube furnace, respectively. Then the furnace was heated to 300 °C at a rate of 2 °C min⁻¹ and maintained at 300 °C for 2 h with a continuous flow of N₂. The NF/CoP was thus harvested.

Materials characterization

X-ray powder diffraction (XRD) was acquired from Bruker D8 advance system with a scanning rate of $10^\circ \text{ min}^{-1}$ (Cu K_α radiation). The scanning range was from 3° to 80° . The X-ray photoelectron spectroscopy (XPS) was performed on Thermo ESCALAB 250 X-ray photoelectron spectrometer. The binding energy of the C 1s peak (284.8 eV, C-C bond) was used as the internal standard. The scanning electron microscopy (SEM) was performed using Zeiss Sigma 500 electron microscope with an energy-dispersive X-ray spectroscopy (EDS) analyzer. Transmission electron microscope (TEM) images, high resolution (HR-) TEM were respectively obtained via FEI Tecnai G2 Spirit operated at 120 kV and FEI Tecnai G2 F30 at 300 kV. The Fourier transform infrared (FTIR) spectra were carried out in Nicolet™ iS50 FTIR spectrometer (Thermo Fisher, USA) between 4000 and 400 cm^{-1} .

In-situ Raman measurements

In-situ electrochemical Raman spectra were performed on a confocal Raman microspectrometer (Renishaw inVia Qontor, UK) using a 785 nm laser and the applied potentials were adjusted by a CHI 760E electrochemical workstation equipped with an in-situ Raman spectroelectrochemical cell. During the in-situ Raman measurement, $\text{Ni}(\text{OH})_2\text{-adp}$ served as the working electrode, Ag/AgCl electrode served as the reference electrode, and graphite rod served as the counter electrode.

Electrochemical measurements

All Electrochemical measurements were carried out on an electrochemical workstation (Autolab, PGSTAT 302N) with a standard three-electrode configuration using a graphite rod as the counter electrode, a Hg/HgO (filled with 1 M KOH solution) electrode as the reference electrode, and a piece of our prepared sample ($1 \times 1 \text{ cm}^2$) as the working electrode. The electrolytes used in this work were 1 M KOH and 1 M KOH + 0.1 M EG at room temperature. The electrochemical measurements were carried out at least on four working electrodes to assess the reproducibility and their average was taken into account. All potentials mentioned in measurement were calibrated to the reversible hydrogen electrode (RHE) scale according to the Nernst equation: $E (\text{RHE}) = E (\text{Hg}/\text{HgO}) + 0.098 + 0.0591 \times \text{pH}$. Prior to each measurement, all the working electrodes were treated by cyclic voltammetry (CV) scans from 1.2 to 1.6 V vs. RHE several times at a scan rate of 50 mV s^{-1} until the signals were relatively stabilized. Linear sweep voltammetry (LSV) was performed with a scan rate of 5 mV s^{-1} to obtain the polarization curves. All the polarization curves were corrected with 95% iR-compensation.

Electrochemical impedance spectroscopy (EIS) was measured in the frequency range from 10^5 Hz to 10^{-2} Hz . The electrochemical double-layer capacitance (C_{dl}) of the samples was measured from CV curves in a non-Faradaic potential range of 1.05 - 1.10 V vs. RHE with different scan rates of 20, 40, 60, 80, and 100 mV s^{-1} . The plot of current density difference ($j_a - j_c$) against the scan rate has a linear relationship and its slope is equivalent to twice of the C_{dl} .

The formate productivity and FE of NF/(OH)₂ and NF/(OH)₂-adp at different potentials (1.35-

1.55 V vs. RHE) were investigated by 2 h chronoamperometry (CA) test in 1 M KOH + 0.1 M EG.

The dynamic process of EGOR over NF/Ni(OH)₂-adp at 1.45 V vs. RHE was performed by CA measurement without iR-compensation in 25 mL electrolyte solution of 1 M KOH + 0.01 M EG.

The stability test of the NF/(OH)₂-adp was performed by multiple CA measurement without iR-compensation in 25 mL electrolyte solution of 1 M KOH + 0.1 M EG. The potential was set at 1.45 V vs. RHE.

For the two-electrode integrated electrolyzer, the NF/(OH)₂-adp was used as the anode, and the previously reported high-performing NF/CoP was used as the cathode. The electrocatalytic performance was evaluated in 70 mL electrolyte solution of 1 M KOH + 0.1 M PET.

Electrochemical adsorbate-stripping measurement was carried out by immersing the electrode in 1 M KOH + 0.1 M EG at 0.2 V vs. RHE for 1 min to adsorb EG. Then the electrode was rinsed with deionized water to remove excess EG and transferred to the electrochemical cell containing 1 M KOH for the electro-oxidation stripping of the adsorbed EG by LSV (1.0-1.6 V vs. RHE) for 5 scans. The oxidation charge Q_{Ox} involved in the process was calculated by the sum of stripping charges of each scan minus the last scan, as shown in equation S1.

$$Q_{Ox} = \sum_{i=1}^5 (Q_i - Q_5) \quad (S1)$$

where Q_i ($i = 1 - 5$) is the stripping charge of each LSV scan.

Product analysis

The products of EGOR were quantified by high performance liquid chromatography (HPLC, Shimadzu LC-16) equipped with an organic acid column (Coregel 87H3, 55 °C), ultraviolet detector (210 nm), and differential refractive index detector. The mobile phase was 8 mM H₂SO₄ aqueous solution with a flow rate of 0.6 mL min⁻¹. In addition, the products were confirmed by ¹H nuclear magnetic resonance spectroscopy (¹H NMR, Bruker AVANCE NEO 500).

The conversion of EG can be calculated according to equation S2:

$$\text{Conversion (EG) (\%)} = \frac{n(\text{reacted EG})}{n(\text{initial EG})} \times 100\% \quad (\text{S2})$$

The yields of glycolic acid (GA) and formate can be calculated according to equation S3 and S4:

$$\text{Yield (GA) (\%)} = \frac{n(\text{GA production})}{n(\text{initial EG})} \times 100\% \quad (\text{S3})$$

$$\text{Yield (formate) (\%)} = \frac{n(\text{formate production})}{2 \times n(\text{initial EG})} \times 100\% \quad (\text{S4})$$

The productivity of formate can be calculated according to equation S5:

$$\text{Productivity (formate) (mmol cm}^{-2} \text{ h}^{-1}) = \frac{n(\text{formate production})}{S \times T} \quad (\text{S5})$$

where S is area of anode (cm²), T is reaction time (h).

The selectivity of formate can be determined by equation S6:

$$\text{Selectivity (formate) (\%)} = \frac{n(\text{formate production})}{n(\text{GA production} + \text{formate production})} \times 100\% \quad (\text{S6})$$

The Faradaic efficiency of formate can be calculated using equation S7:

$$\text{Faradaic efficiency (\%)} = \frac{nzF}{It} \times 100\% \text{ (S7)}$$

where n is the mole of the formate (mol), z is the number of electrons transferred (for the formate, $z = 3$), F is the Faradaic constant (96485 C mol^{-1}), I is the current (A), and t is the potentiostatic test time (s).

Hydrolysis of PET

The PET plastic bottles [cestbon, China Resources C'estbon Beverage (China) Co. Ltd.] (sliced into small pieces) were pretreated with ethanol and deionized water each for 5 min. For the depolymerization of PET, 2 g of PET plastic bottles and 50 mL of 2 M KOH aqueous solution were transferred into a 100 mL Teflon-lined stainless-steel autoclave and heated at $180 \text{ }^\circ\text{C}$ for 2 h to obtain 0.2 M PET in 2 M KOH solution. The reaction of PET depolymerization is proposed as follows:



Computational details

The density functional theory (DFT) calculations were performed using the CASTEP packages.² The generalized gradient approximation method (GGA) with the Perdew-Burke-Ernzerh (PBE) functional was used to describe the exchange and correlation interactions.³ Ultrasoft pseudo-potentials were used to account for core-valance interaction.⁴ A three-layer 1×4 supercell of $\text{Ni}(\text{OH})_2$ (010) surface was constructed to simulate the $\text{Ni}(\text{OH})_2$, and the top layer was allowed to

relax. In the geometric optimization process, the Broyden-Fletcher-Goldfarb-Shanno (BFGS) scheme was chosen as the minimization algorithm. The Monkhorst-Pack scheme K-points grid sampling was set as $2 \times 2 \times 1$ for the irreducible Brillouin zone. The electronic wave functions were expanded on a plane wave basis with a cut-off energy of 400 eV and the self-consistent field (SCF) tolerance was 1×10^{-5} eV. The optimization would accomplish when the energy, maximum force, maximum stress and maximum displacement were less than 1.0×10^{-4} eV/atom, 0.03 eV/Å, 0.05 GPa, and 0.001 Å, respectively. To eliminate contact between two periodic units, a vacuum slab with a thickness of 15 Å was used in the z-direction. The adsorption energy (E_{ads}) between the surface and molecule is determined by the following equation: $E_{\text{ads}} = E_{\text{molecule+surface}} - E_{\text{molecule}} - E_{\text{surface}}$, where $E_{\text{molecule+surface}}$, E_{molecule} , and E_{surface} are the energy of adsorbate molecule adsorbed on the surface, the energy of molecule, and the energy of clean surface, respectively.

Regarding the EGOR, the Gibbs free energy for each step can be calculated by the following equation:

$$\Delta G = \Delta E + \Delta ZPE - T\Delta S$$

where ΔE represents the energy difference between products and reactants calculated from DFT; ΔZPE represents the zero-point energy change, ΔS represents the entropy change for each reaction.

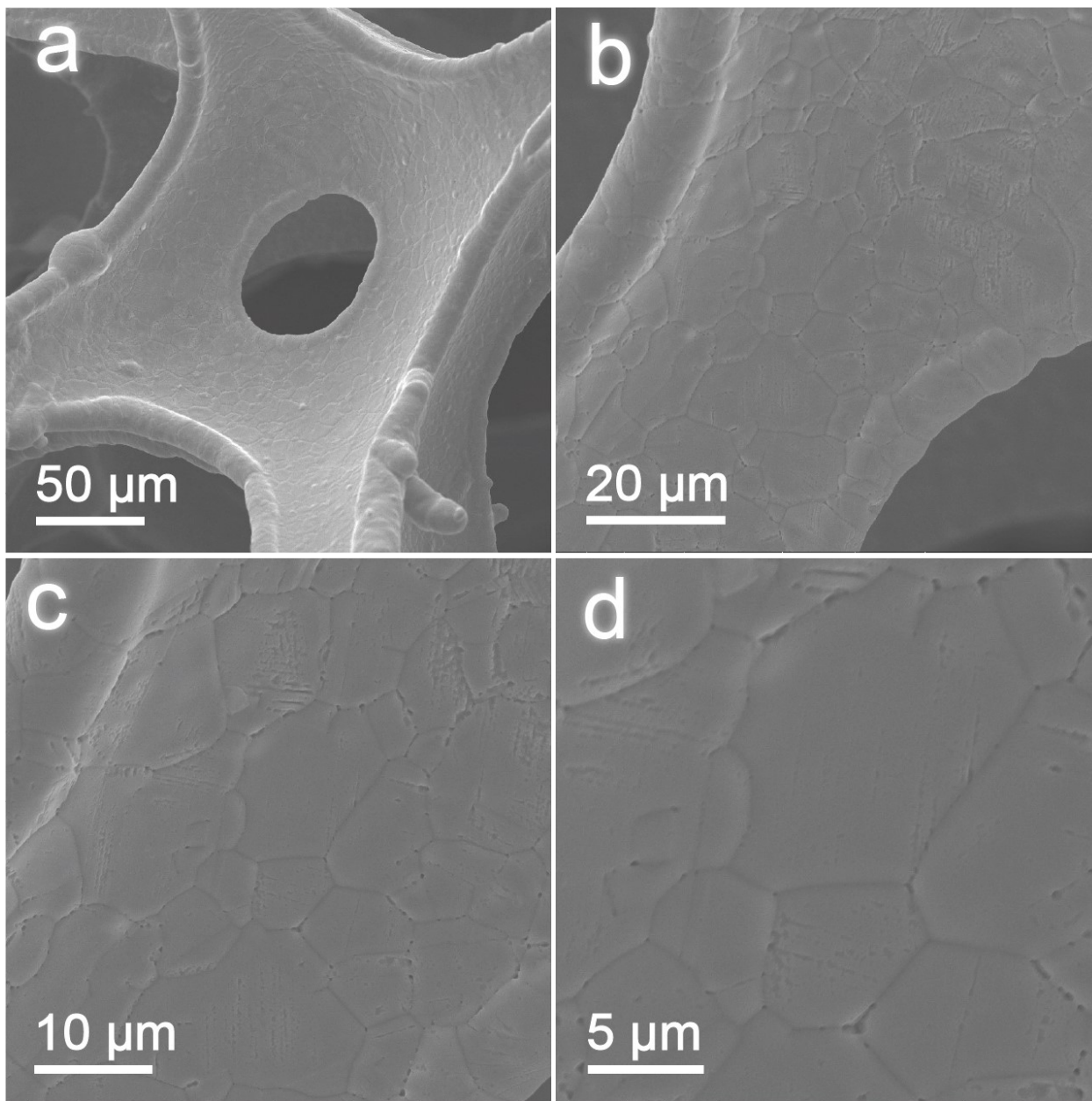


Figure S1. (a-d) SEM images of NF.

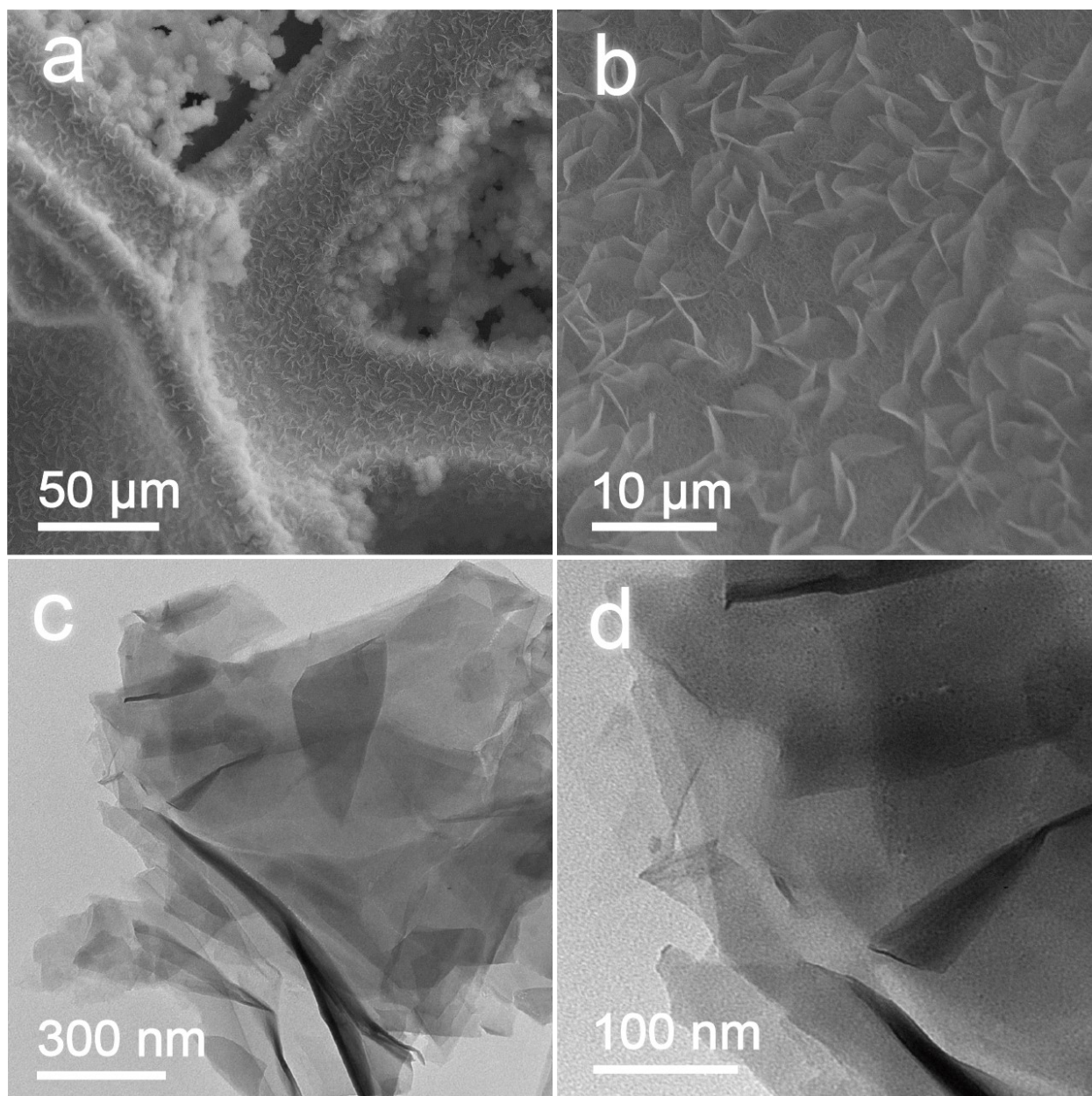


Figure S2. (a,b) SEM and (c,d) TEM images of the NF/Ni(OH)₂.

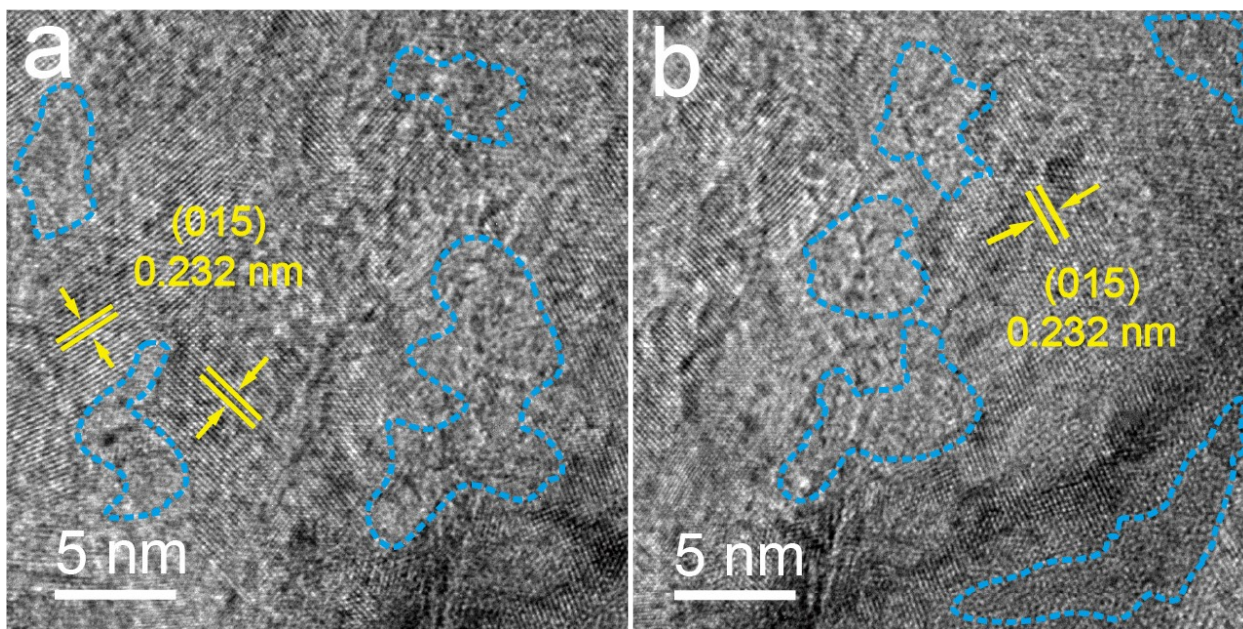


Figure S3. (a,b) HRTEM images of NF/Ni(OH)₂-adp.

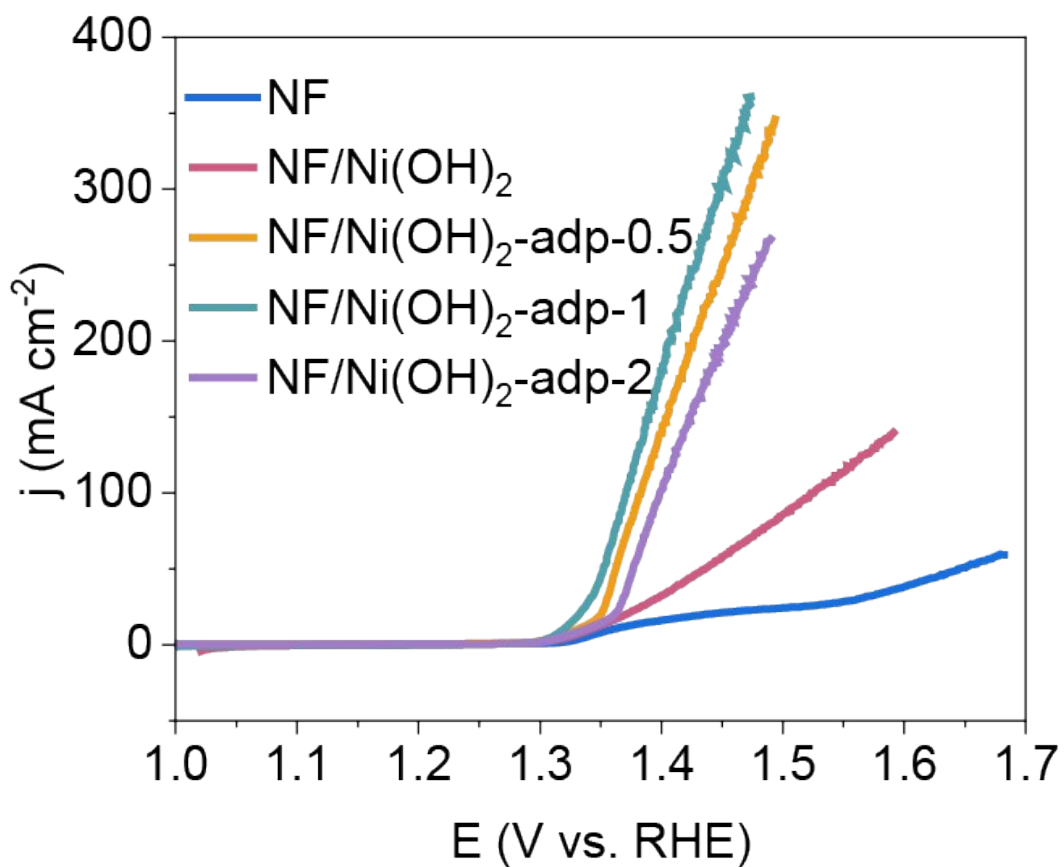


Figure S4. Polarization curves of NF, NF/Ni(OH)₂, and NF/Ni(OH)₂-adp-x (x = 0.5, 1, and 2) tested in 1 M KOH + 0.1 M EG.

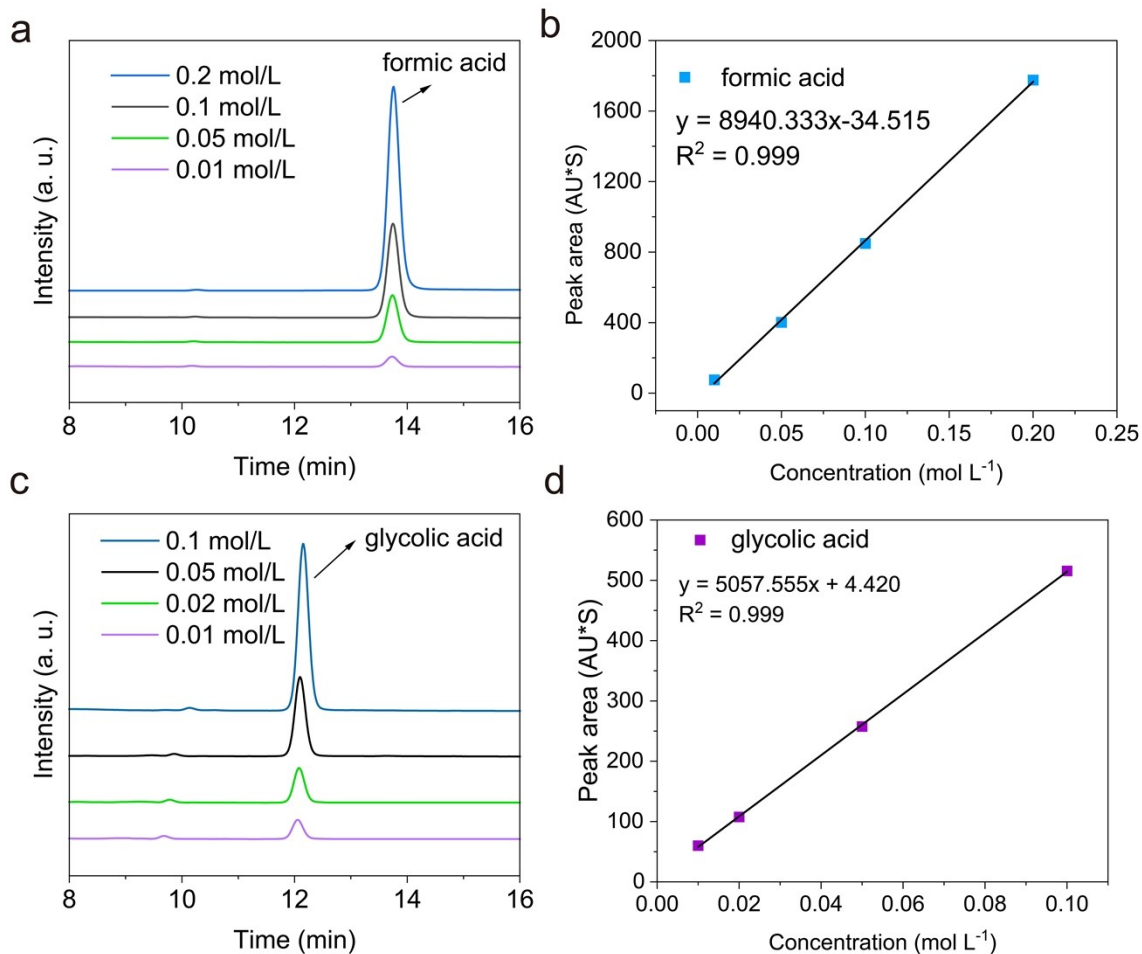


Figure S5. (a) HPLC spectra and (b) the corresponding standard curves of formic acid. (c) HPLC spectra and (d) the corresponding standard curves of glycolic acid.

Note: The standard solutions of formic acid (0.01, 0.05, 0.1, and 0.2 mol/L) and glycolic acid (0.01, 0.02, 0.05, and 0.1 mol/L) were prepared. All standards were dissolved in 1 M KOH as the reaction solution to eliminate matrix effect interference. The calibration curve was established by using the peak areas and concentrations of the standard samples.

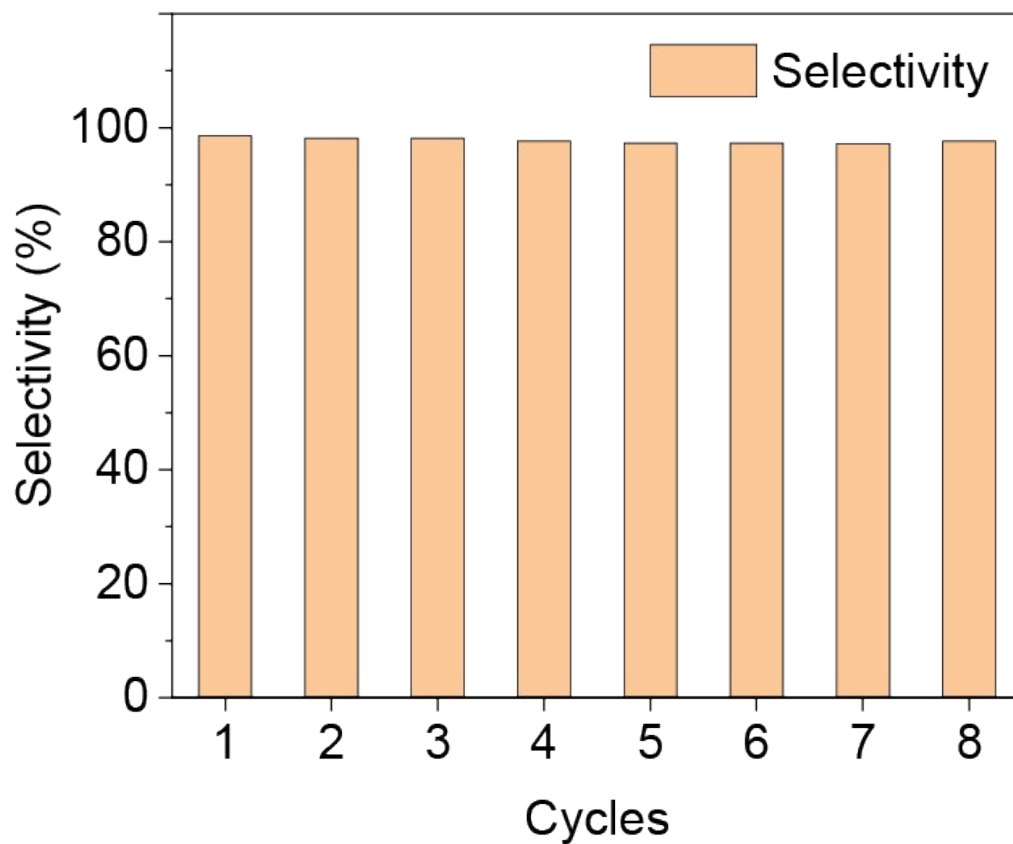


Figure S6. Stability test of NF/Ni(OH)₂-adp in 1 M KOH + 0.1 M EG at 1.45 V vs. RHE: the selectivity of formate for 8 cycles.

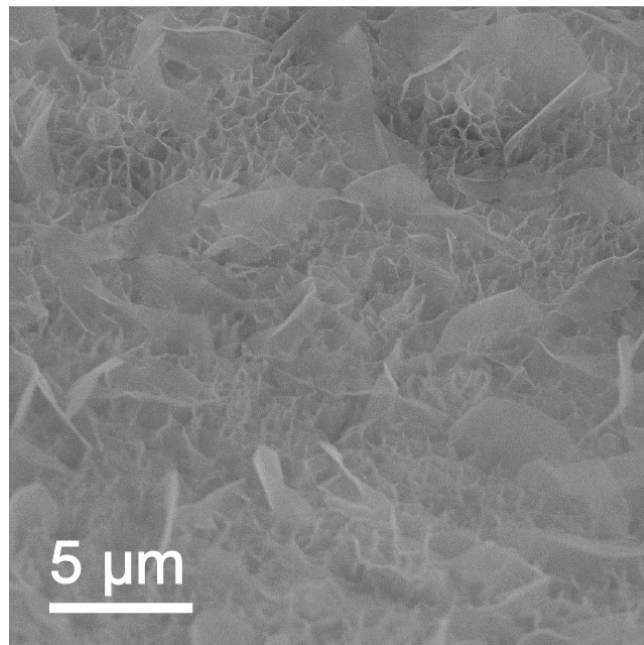


Figure S7. SEM image of the used NF/Ni(OH)₂-adp.

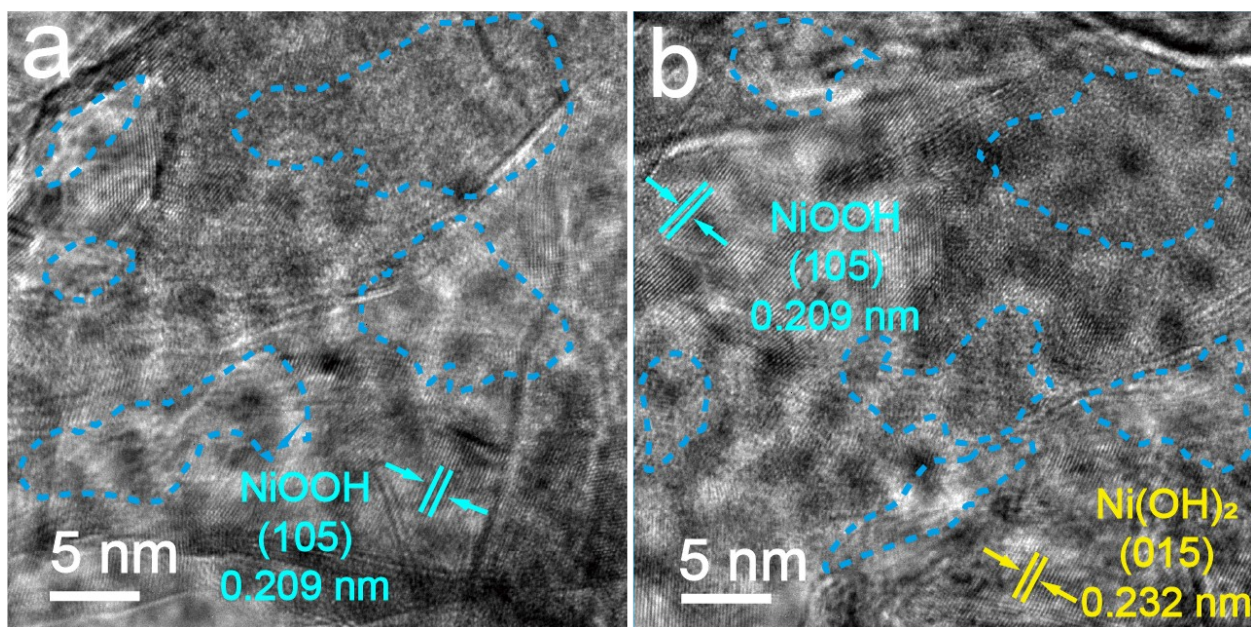


Figure S8. (a,b) HRTEM images of the used NF/Ni(OH)₂-adp.

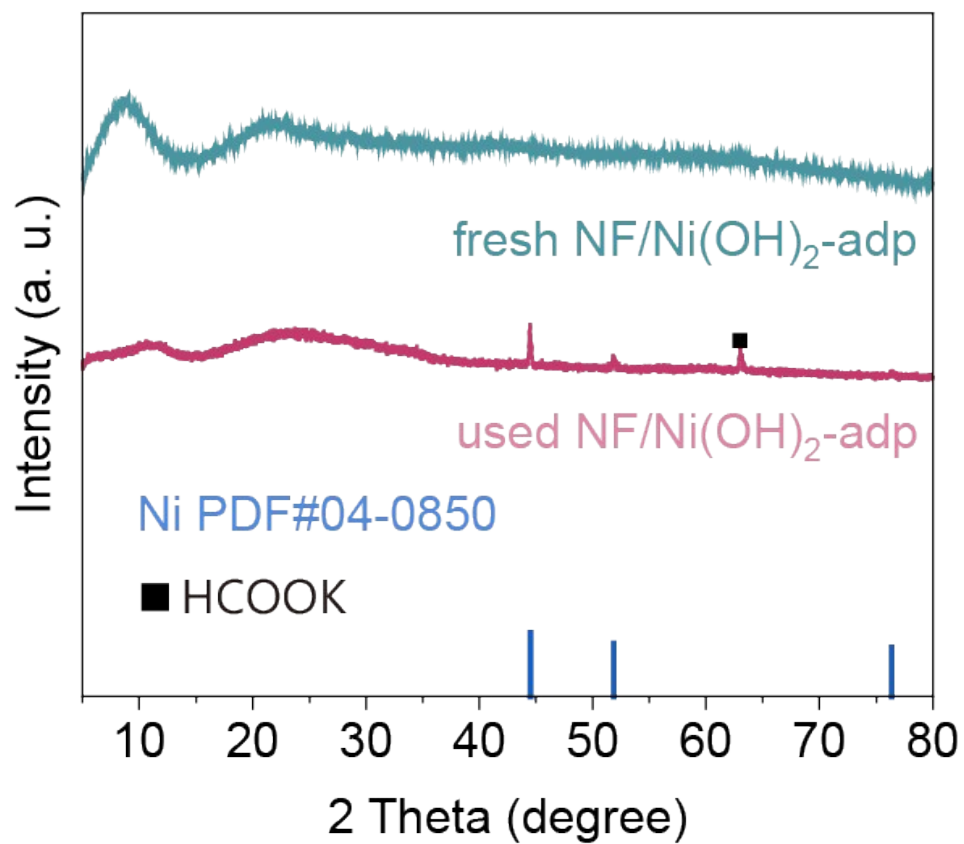


Figure S9. The XRD pattern of the used NF/Ni(OH)₂-adp. For comparison, the XRD pattern of the fresh one is also shown.

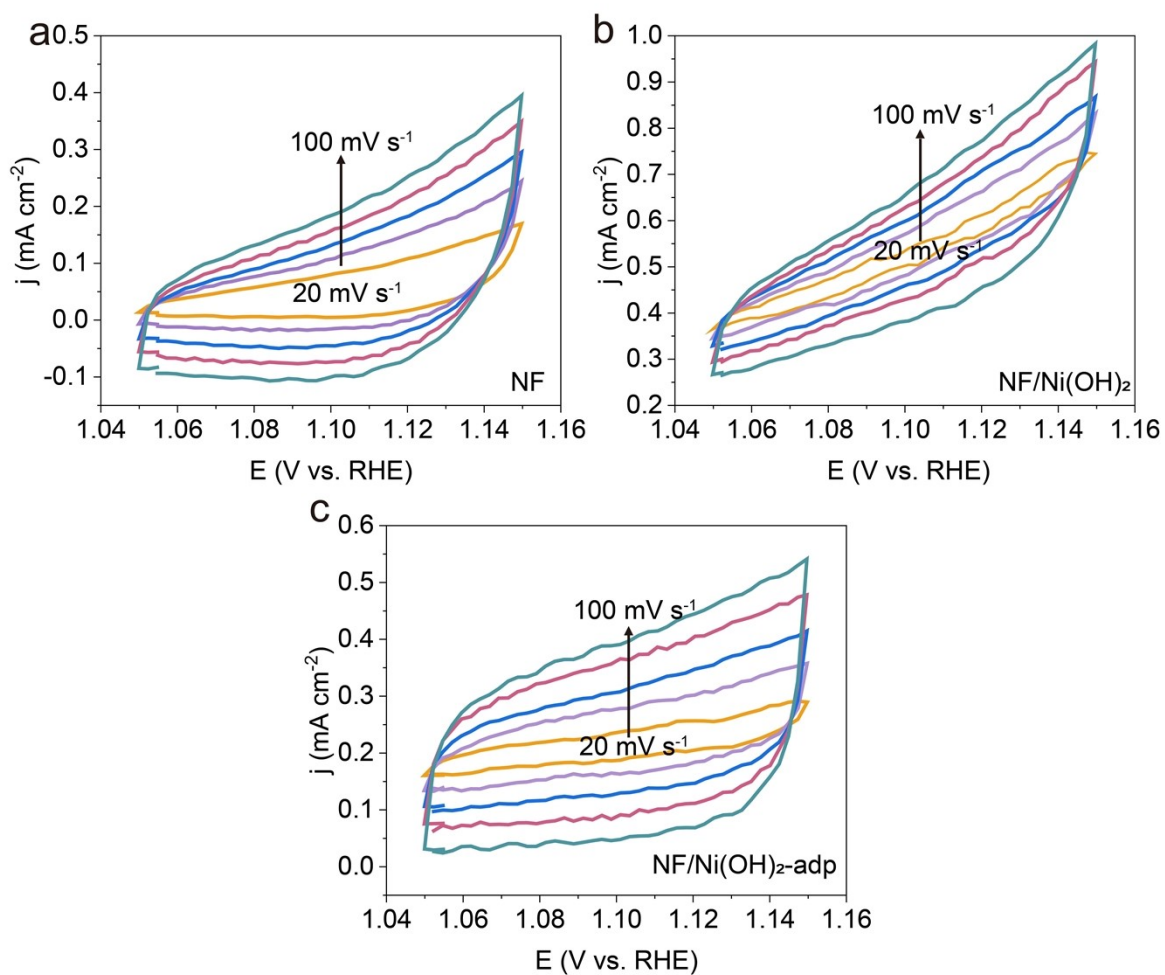


Figure S10. CV curves of (a) NF, (b) NF/Ni(OH)₂, and (c) NF/Ni(OH)₂-adp obtained at 1.05-1.10 V vs. RHE with different scanning rates (20, 40, 60, 80, and 100 mV s⁻¹).

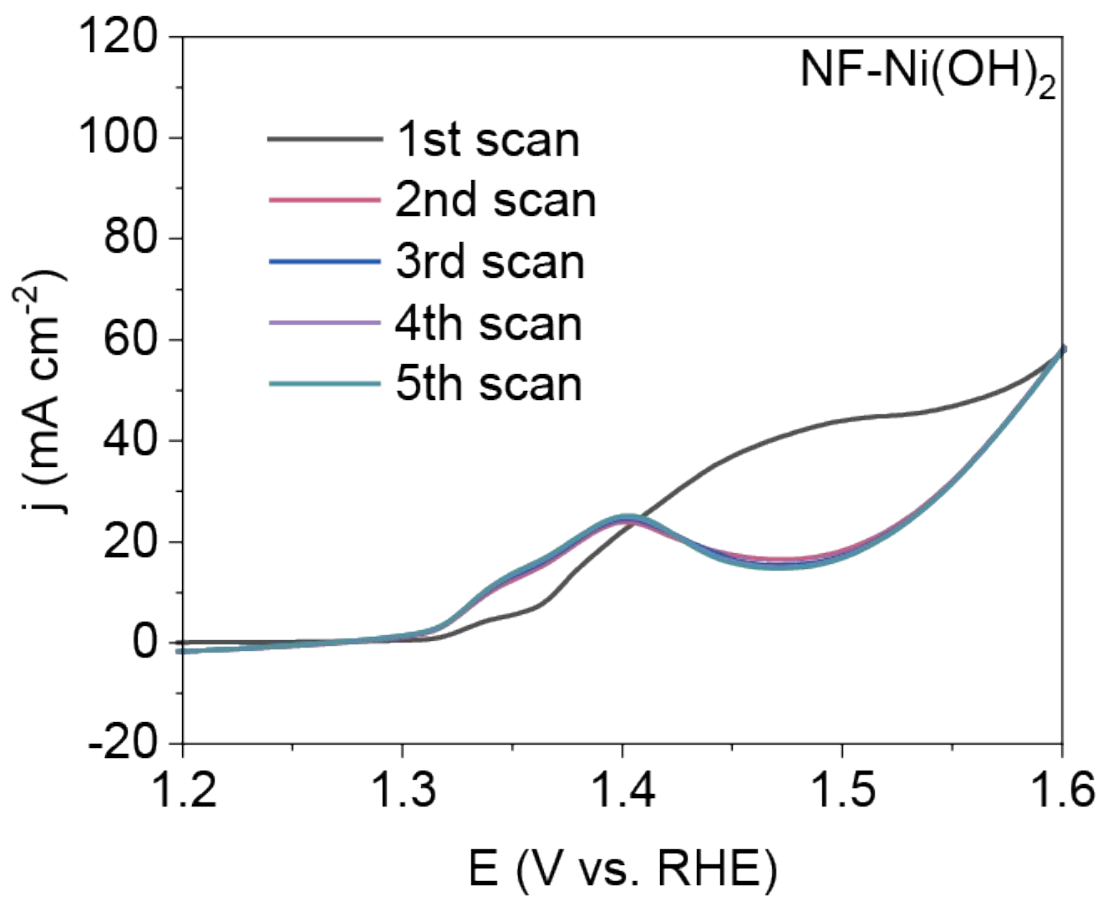


Figure S11. Electrochemical adsorbate-stripping curves of NF/Ni(OH)₂.

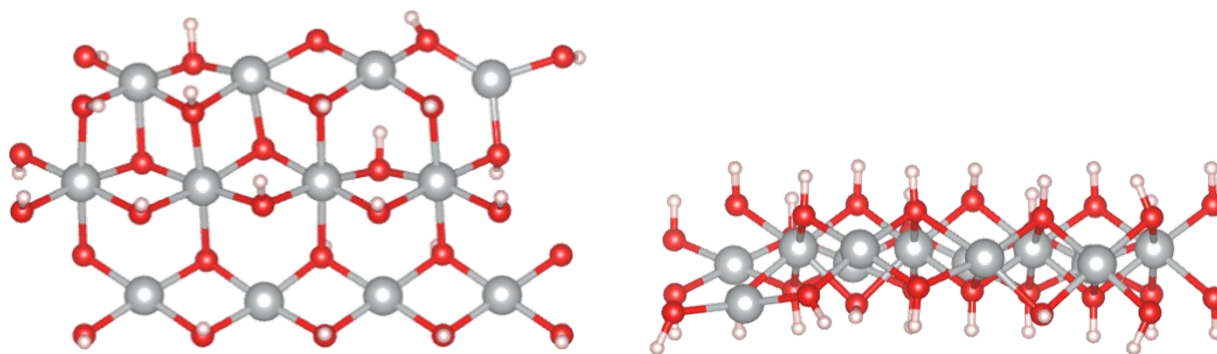


Figure S12. Optimized structure slab of $\text{Ni}(\text{OH})_2$ for DFT calculations. The gray, red, brown, and pink spheres refer to the Ni, O, C, and H atoms, respectively.

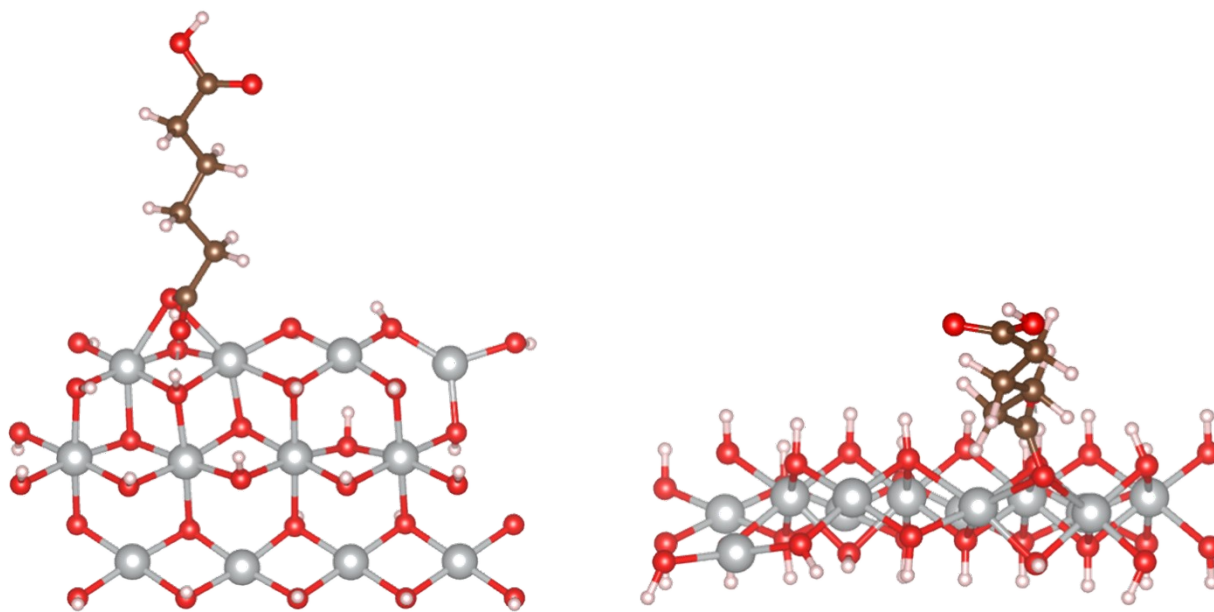


Figure S13. Optimized structure slab of Ni(OH)₂-adp for DFT calculations.

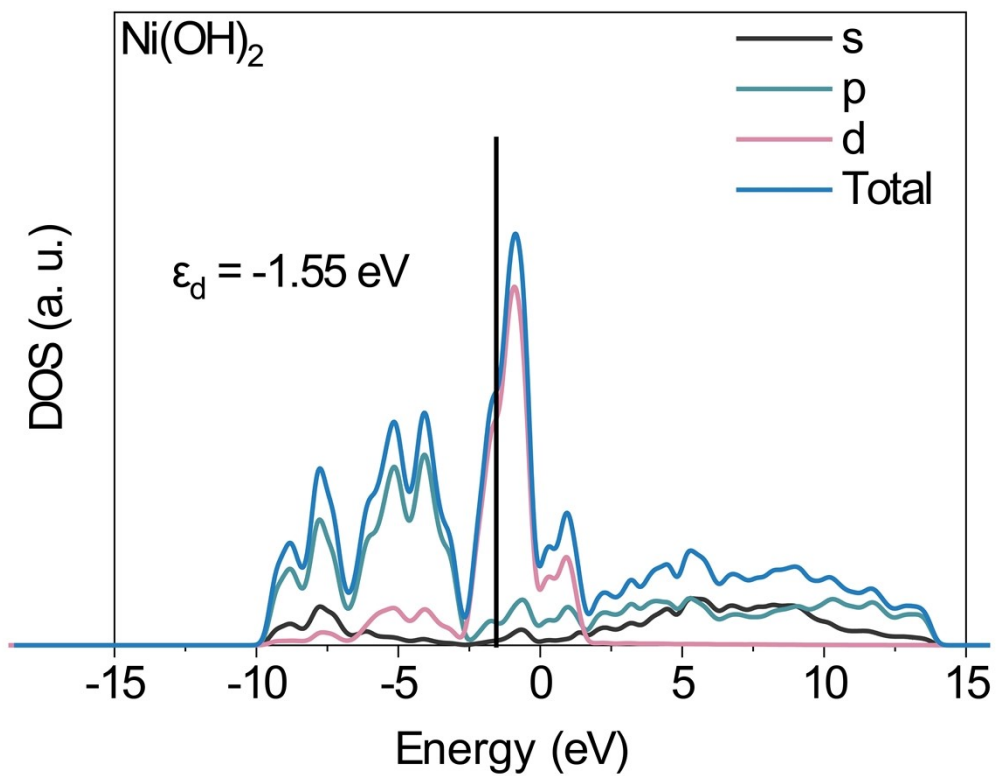


Figure S14. Calculated DOS of Ni(OH)₂.

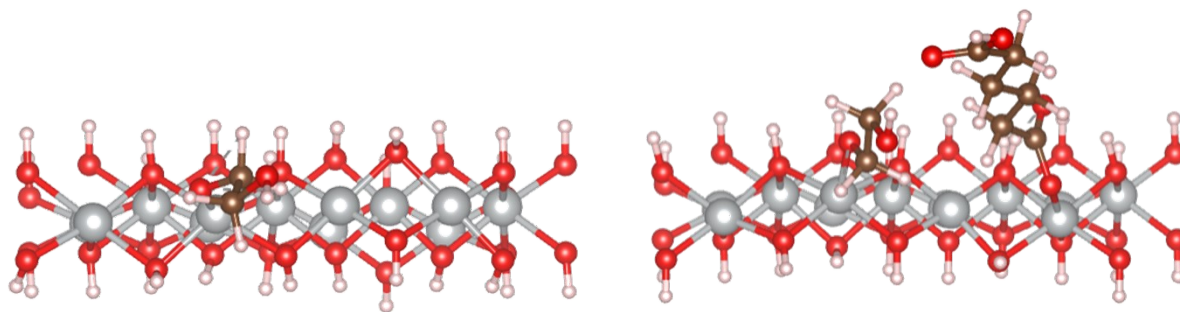


Figure S15. The optimized configurations for EG adsorption on $\text{Ni}(\text{OH})_2$ and $\text{Ni}(\text{OH})_2\text{-adp}$.

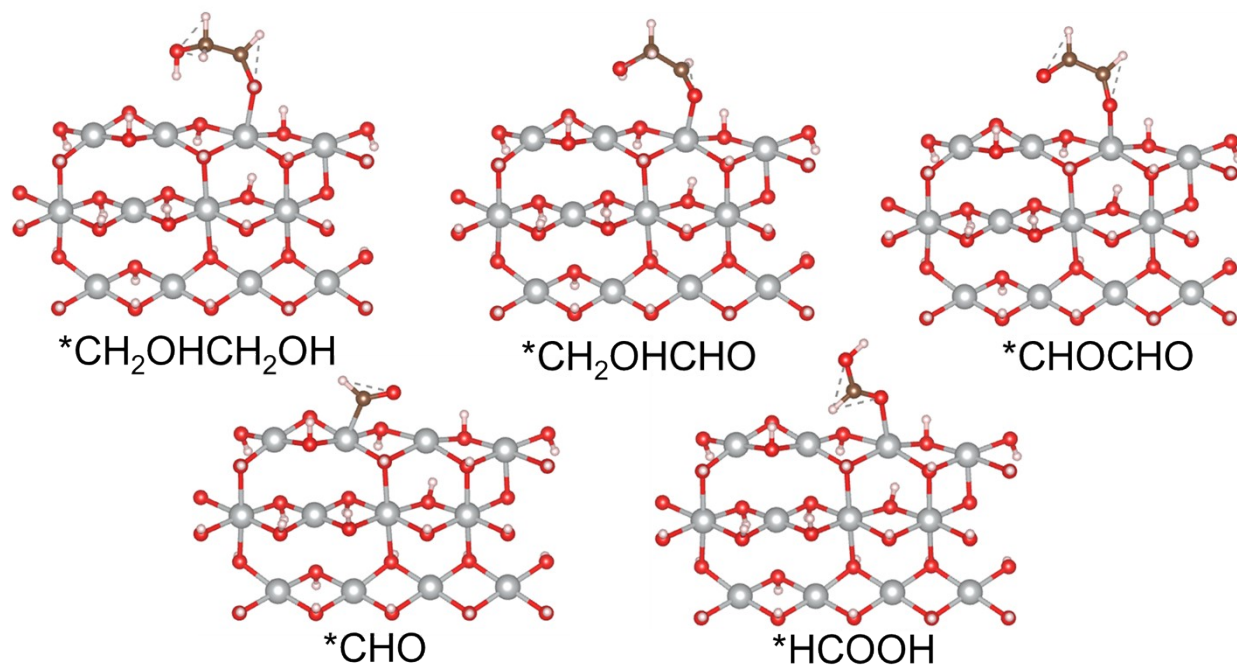


Figure S16. The intermediate adsorption structural models for EGOR on Ni(OH)₂.

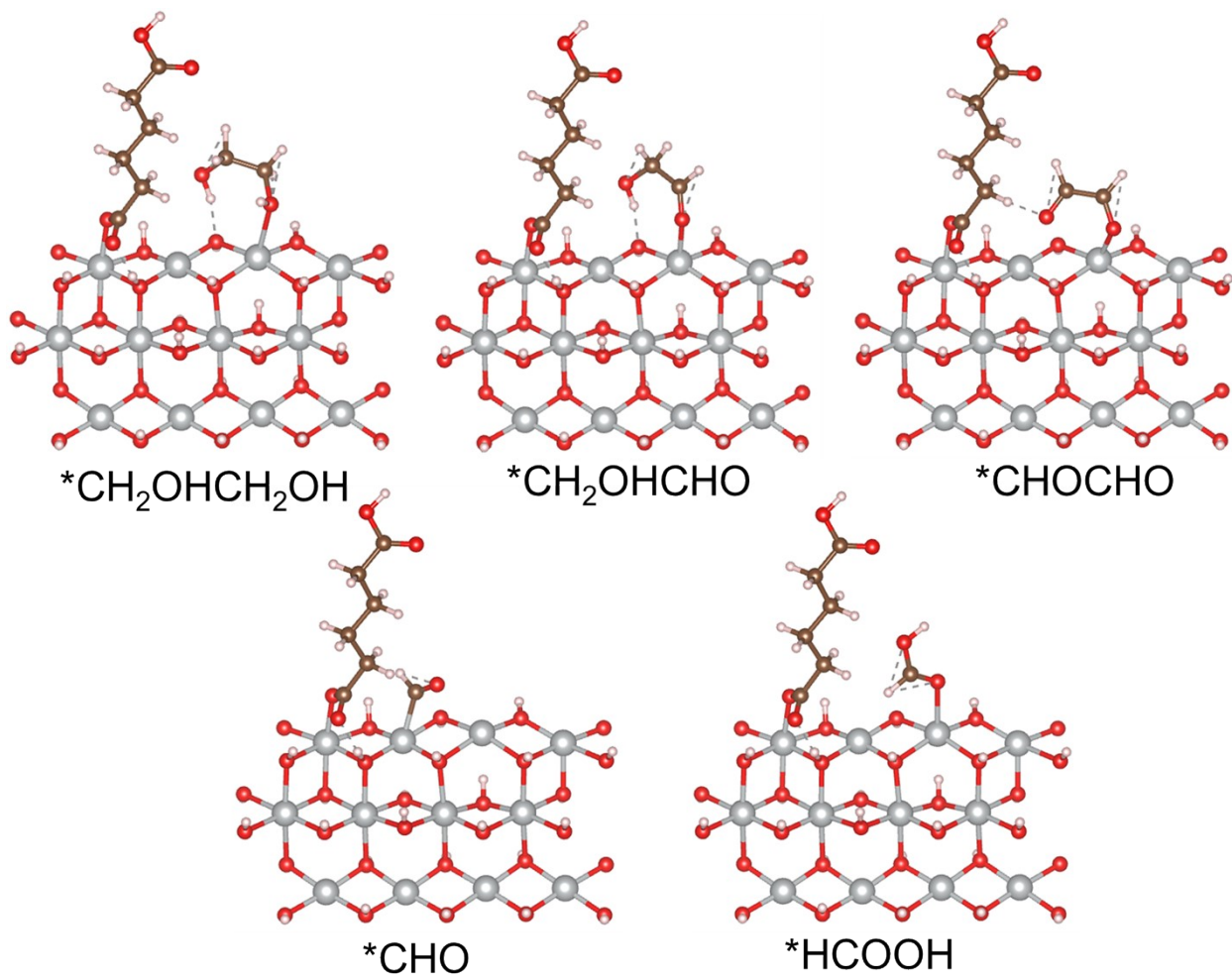


Figure S17. The intermediate adsorption structural models for EGOR on Ni(OH)₂-adp.

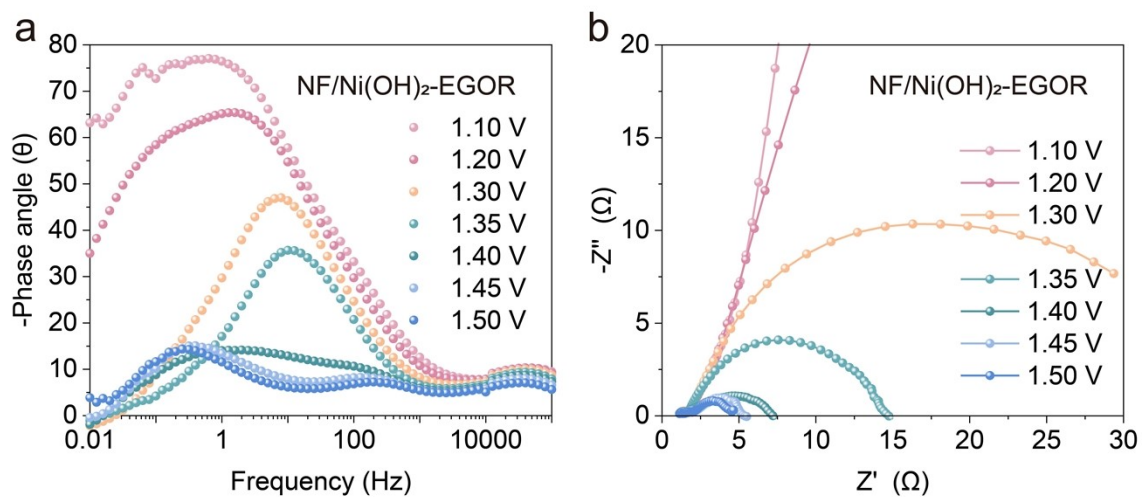


Figure S18. (a) Bode phase plots and (b) Nyquist plots of the NF/Ni(OH)₂ at potentials from 1.10 V to 1.50 V vs. RHE in 1 M KOH + 0.1 M EG.

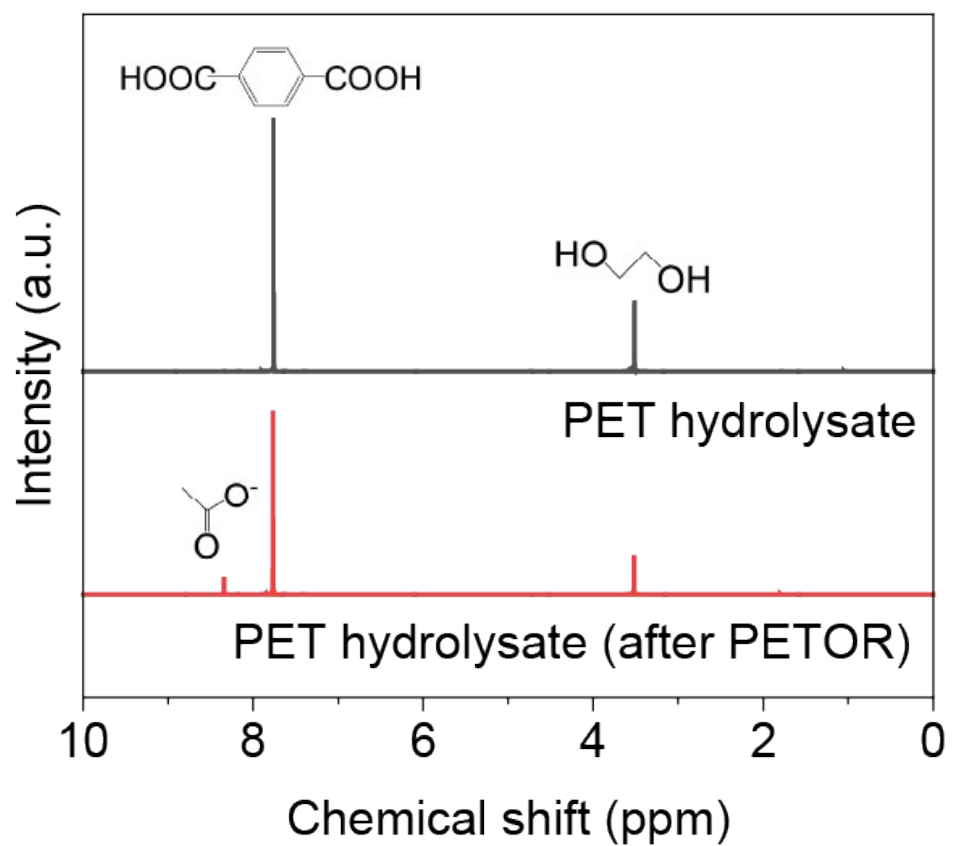


Figure S19. ¹H NMR spectra for fresh PET hydrolysate and PET hydrolysate after electro-oxidation reaction (PETOR).

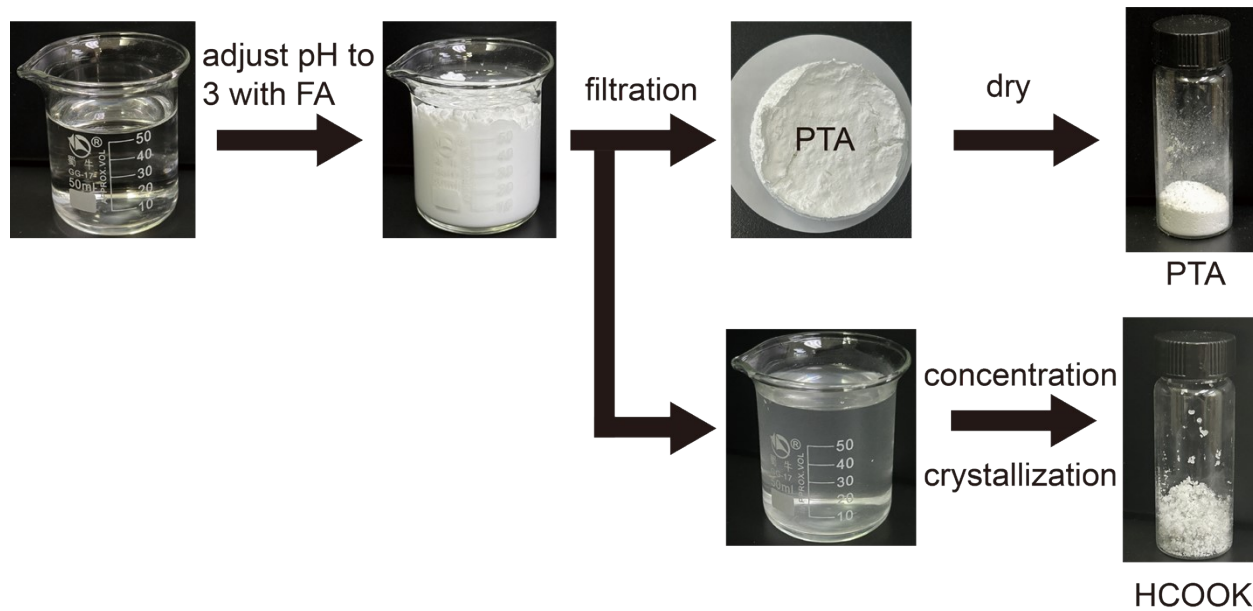


Figure S20. Procedure of product separation from PET hydrolysate after electro-oxidation reaction (PETOR).

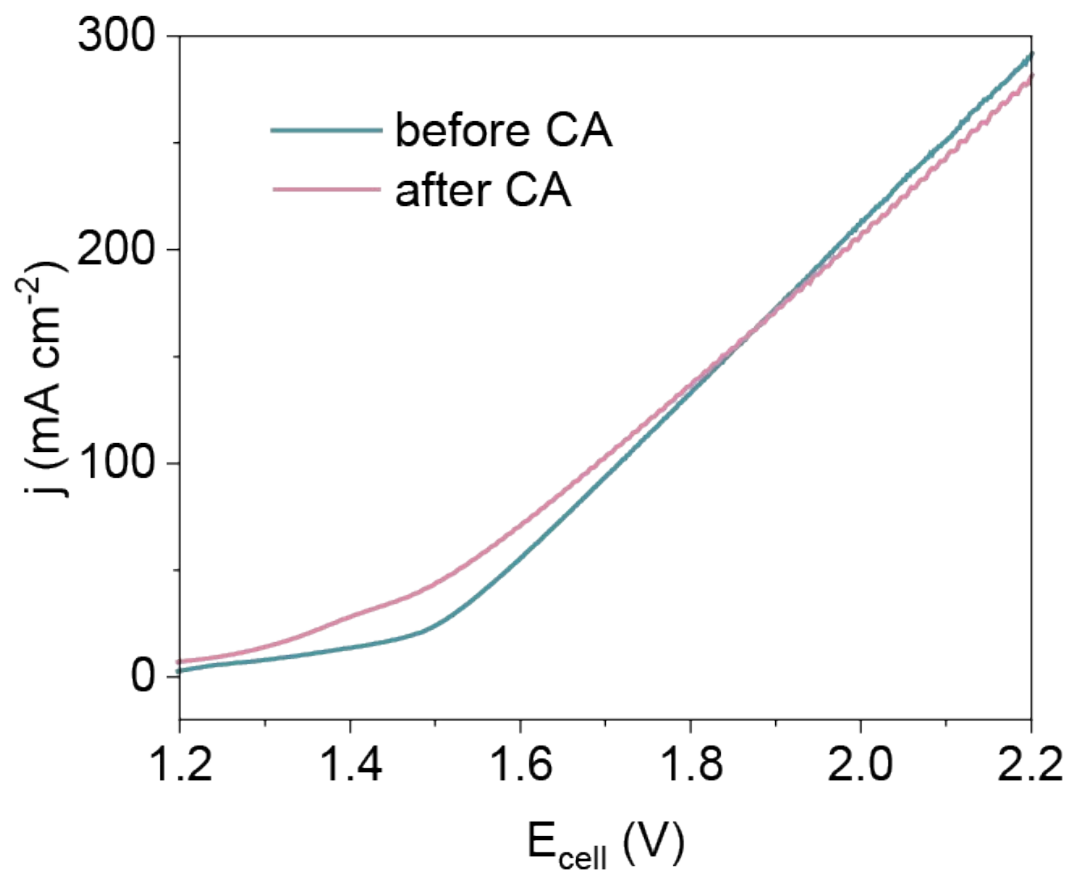


Figure S21. HER||PETOR polarization curve after long-term CA stability test.

Table S1. Comparison of the electrocatalytic EGOR performance of our proposed NF/Ni(OH)₂-adp with other recently reported EGOR catalysts.

Catalyst	Electrolyte	E (V)@10/50 (mA/cm²)	Tafel slope (mV dec⁻¹)	FE (%)	Ref.
NF/Ni(OH)₂-adp	1 M KOH + 1 M EG	1.32@10 1.35@50	30.2	98.2 (1.35 V)	This work
NiMnLDH	1 M KOH + 1 M EG	1.37@10	207.0	85.8 (~ 1.4 V)	5
NF/NiCu _{60s}	1 M KOH + 0.3 M EG	1.36@10	31.1	95.8 (1.47 V)	6
CFP/NiCo ₂ O ₄	1 M KOH + 0.1 M PET	1.35@10 1.44@50	96.0	93 (1.45 V)	7
OMS-Ni ₁ -CoP	1 M KOH + 0.5 M EG	1.38@50	108.0	96 (1.3 V)	8
Cobalt-Based Coordination Polymer	1 M KOH + 0.1 M EG	1.42@10	117.0	-	9
Ni ₃ N/W ₅ N ₄	PET hydrolysate	1.33@10	-	85 (1.5 V)	10
NF/Pd NTs	PET hydrolysate	1.58@50	-	81.17 ± 2.7 (1.5 V)	11

Catalyst	Electrolyte	E (V)@10/50 (mA/cm ²)	Tafel slope (mV dec ⁻¹)	FE (%)	Ref.
CF/CuO NWs	PET hydrolysate	1.38@10	96.0	-	12
Mn _{0.1} Ni _{0.9} Co ₂ O _{4-δ} RSFs	1 M KOH + 0.17 M EG	1.51@50	224.0	95 (1.42 V)	13
GC/NiSe ₂	1 M KOH + 1 M EG	1.389@10	-	-	14

Note:

All the potentials are vs. RHE.

“~” represents the estimated value from the corresponding figure.

REFERENCE

1. L. Zeng, Y. Chen, M. Sun, Q. Huang, K. Sun, J. Ma, J. Li, H. Tan, M. Li, Y. Pan, Y. Liu, M. Luo, B. Huang and S. Guo, *J. Am. Chem. Soc.*, 2023, **145**, 17577-17587.
2. S. J. Clark, M. D. Segall, C. J. Pickard, P. J. Hasnip, M. I. J. Probert, K. Refson and M. C. Payne, *Z. Krist. Cryst. Mater.*, 2005, **220**, 567-570.
3. B. Delley, *J. Chem. Phys.*, 1990, **92**, 508-517.
4. D. Vanderbilt, *Phys. Rev. B*, 1990, **41**, 7892-7895.

5. Z. Wang, J. Li, Q. Zhang, C. Wu, H. Meng, Y. Tang, A. Zou, Y. Zhang, R. Ma, X. Lv, Z. Yu, S. Xi, J. Xue, X. Wang and J. Wu, *Angew. Chem. Int. Ed.*, 2024, **63**, e202411517.
6. H. Kang, D. He, X. Yan, B. Dao, N. B. Williams, G. I. Elliott, D. Streater, J. Nyakuchena, J. Huang, X. Pan, X. Xiao and J. Gu, *ACS Catal*, 2024, **14**, 5314-5325.
7. J. Wang, X. Li, M. Wang, T. Zhang, X. Chai, J. Lu, T. Wang, Y. Zhao and D. Ma, *ACS Catal.*, 2022, **12**, 6722-6728.
8. N. Wang, X. Li, M.-K. Hu, W. Wei, S.-H. Zhou, X.-T. Wu and Q.-L. Zhu, *Appl. Catal., B*, 2022, **316**, 121667.
9. S. Behera, S. Dinda, R. Saha and B. Mondal, *ACS Catal.*, 2023, **13**, 469-474.
10. F. Ma, S. Wang, X. Gong, X. Liu, Z. Wang, P. Wang, Y. Liu, H. Cheng, Y. Dai, Z. Zheng and B. Huang, *Appl. Catal., B*, 2022, **307**, 121198.
11. T. Ren, Z. Duan, H. Wang, H. Yu, K. Deng, Z. Wang, H. Wang, L. Wang and Y. Xu, *ACS Catal.*, 2023, **13**, 10394-10404.
12. J. Wang, X. Li, T. Zhang, Y. Chen, T. Wang and Y. Zhao, *J. Phys. Chem. Lett.*, 2022, **13**, 622-627.
13. Y. Mao, S. Fan, X. Li, J. Shi, M. Wang, Z. Niu and G. Chen, *Journal of Hazardous Materials*, 2023, **457**, 131743.
14. K. Liu, Y. Wang, F. Liu, C. Liu, R. Shi and Y. Chen, *Chem. Eng. J.*, 2023, **473**, 145292.